Thermal Science and Engineering (2023) Volume 6 Issue 2
doi: 10.24294/tse.v6i2.3968

ORIGINAL RESEARCH ARTICLE

Numerical study of electrically conducting MHD fluids in a vertical channel with Jeffrey fluid flow and first order chemical reaction

Shreedevi Kalyan[1,*], Jumanne Mng'ang'a[2]

[1] *Department of Mathematics, Sharnbasva University, Kalaburagi 585103, Karnataka, India.*

[2] *The Local Government Training Institute, P.O. BOX 1125, Dodoma, Tanzania.*

*** Corresponding author:** Shreedevi Kalyan, kalyanshreedevi@gmail.com

ABSTRACT

This research paper explores the influence of first-order chemical reactions on the sustainable properties of electrically conducting magnetohydrodynamic (MHD) fluids in a vertical channel with the unique characteristics of Jeffrey fluid flow. The mathematical model of MHD flow with Jeffrey fluid and chemical reaction incorporates the impacts of viscous dissipation, Joule heating, and a non-Newtonian fluid model with viscoelastic properties in the flow regions. The governing equations of the flow field were solved using the finite difference method, and the impacts of flow parameters on the flow characteristics were discussed numerically using a graphical representation. It's revealed that increasing the Jeffrey parameter results in a decline in the velocity field profiles. Also, species concentration field profiles decline with higher values of the destruction chemical reaction parameter. The findings of this study have significant implications for various engineering applications, including energy generation, aerospace engineering, and material processing. Additionally, the inclusion of Jeffrey's fluid flow introduces a viscoelastic component, enhancing the complexity of the fluid dynamics.

Keywords: magnetohydrodynamics; electrically conducting fluids; chemical reaction; Jeffrey fluid flow; finite difference

ARTICLE INFO

Received: 14 November 2023
Accepted: 19 December 2023
Available online: 31 December 2023

1. Introduction

Electrically conducting fluids play a crucial role in modern engineering applications, and understanding their behaviour under the influence of magnetic fields is essential for optimizing processes and enhancing sustainability. This paper investigates the sustainability aspects of such fluids by incorporating Jeffrey fluid flow, a non-Newtonian fluid model with viscoelastic properties. Narsimha Reddy et al.[1] studied the behaviour of MHD with Casson fluid and nanofluid for the advanced application of MHD. Magnetohydrodynamics involves the study of the dynamics of electrically conducting fluids, considering the interactions between fluid motion and electromagnetic fields.

First-order chemical reactions, characterized by their rate directly proportional to the concentration of a single reactant, are fundamental in chemical kinetics. The study of these reactions becomes even more compelling when coupled with the complexities introduced by MHD. Electrically conducting fluids, often encountered in plasmas and liquid metals, exhibit unique responses to magnetic fields, leading to phenomena such as magnetohydrodynamic instabilities and magnetic damping. Incorporating first-order chemical reactions into this MHD framework adds an additional layer of intricacy to the understanding of dynamic systems. Noh et al.[2] analysed the surface modification of

dielectric materials to change the dipole-dipole interactions under electric fields. Sedki and Qahiti[3] investigated the phenomenon of radiative heat with an unsteady MHD electrically conducting boundary layer of chemically reactive Casson nanofluid flow due to a pored stretchable sheet immersed in a porous medium in the presence of heat generation, thermophoretic force, and Brownian motion. Furthermore, Venkateswarlu et al.[4] introduced a novel theoretical model known as the trihybrid nanofluid (THNF), which demonstrates remarkable thermal conductivity properties to enhance heat transfer in liquids.

MHD is widely acknowledged as a scientific discipline that places significant emphasis on the dynamics of electrically conducting fluids. The field of MHD boasts many industrial applications, such as accelerometers, cooling system designs using liquid metals, crystal growth, flow meters, and MHD power production. In recent years, numerous scholars have undertaken various studies to gain a comprehensive understanding of the profound impact of magnetic fields on HT and liquid flow across various geometric configurations. Guedri et al.[5] analysed EM-THNF flow over a stretching sheet under the influence of Joule heating and viscous dissipation using the HAM method.

Jeffrey fluid flow introduces a viscoelastic component, characterized by a fractional derivative of the stress tensor. The constitutive equations governing Jeffrey fluid flow will be included in the theoretical framework to capture the unique rheological properties of the fluid. The effect of heat and mass transfer on two immiscible fluids between two vertical plates in the presence of a chemical reaction with radiation parameters was studied by Govindarajan and Lakshmipriya[6]. Sandeep et al.[7] investigated the stagnation point flow of MHD Jeffrey nanofluid over a stretching surface with an induced magnetic field and chemical reaction. Raju et al.[8] analyzed the effects of nonlinear thermal radiation on 3D Jeffrey fluid flow over a stretching/shrinking surface in the presence of homogeneous-heterogeneous reactions, non-uniform heat source/sink, and suction/injection. Rashidi et al.[9] performed mixed convective laminar, incompressible flow, and heat analysis transfer of viscoelastic fluid over a permeable wedge with thermal radiation by employing the homotropy analysis method (HAM).

Recently, Kuznetsov and Nield[10] revised the problem[11] by replacing the boundary condition with a more physical one. It is now assumed that there is no normal mass flux at the plate and that the particle fraction value there adjusts accordingly[12]. Hayat et al.[13] studied magnetohydrodynamic (MHD) three-dimensional flow of couple stress nanofluid in the presence of nonlinear thermal radiation. Malvandi et al.[14] examined laminar film-wise condensation of nanofluids over a vertical plate with nanoparticle migration. Hayat et al.[15] discussed the magnetohydrodynamic (MHD) flow of second-grade nanofluid over a nonlinear stretching surface with convective boundary conditions. Halim et al.[16] addressed the stagnation-point flow of Williamson nanofluid towards a horizontal linearly stretching/shrinking sheet. Hayat et al.[17] studied the active and passive controls of Jeffrey nanofluid flow over a nonlinear stretching surface. Shreedevi et al.[18] analysed the Jeffrey fluid flow of two immiscible fluids in the presence of a chemical reaction.

The novelty of this study is to explore the influence of Jeffrey fluid and first-order chemical reactions on the sustainable properties of electrically conducting magnetohydrodynamic (MHD) fluids in a vertical channel with the unique characteristics of a non-Newtonian fluid model with viscoelastic properties by taking into account the impacts of viscous dissipation and Joule heating in the flow regions. The findings of this study have significant implications for various engineering applications, including energy generation, room ventilation, aerospace engineering, thermal insulation, packed beds, fuel combustion, and processing materials.

2. Mathematical formulation

The flow model consists of electrically conducting and Jeffrey fluid in both regions. A fully developed flow with transfer characteristics, the fluid flow depends on y transverse coordinate and the transverse velocity (the velocity in the x-direction) is negligible in this study, as depicted in **Figure 1**. It is assumed that the fluid

moves only due to the hydrostatic pressure. Hydrostatic and osmotic pressures outside the channel are also assumed to be constant (see [19]).

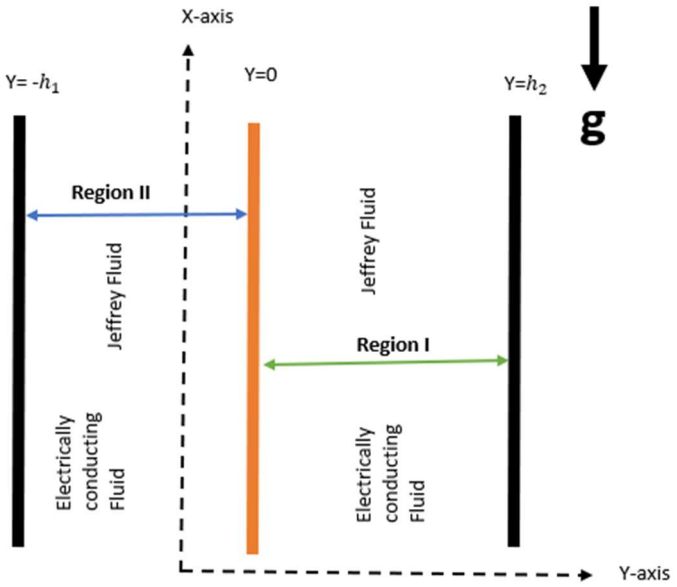

Figure 1. Physical configuration.

The governing equations of the flow problem, including the momentum, energy, and concentration equations, are shown below[18,19]:

Region-I

$$\rho_1\beta_{T1}g(T_1-T_{w2})+\rho_1\beta_{T1}g(C_1-\bar{C}_2)+\frac{\mu_1}{(1+\lambda_1)}\frac{d^2U_1}{dY^2}-\frac{\mu_1U_1}{\kappa}-\frac{dp}{dX}-\sigma_{e1}(E_{01}+B_0U_1)B_0=0$$

$$\frac{d^2T_1}{dY^2}+\frac{\mu_1}{\rho_1\alpha_1C_p}\left(\frac{dU_1}{dY}\right)^2+\frac{\sigma_{e1}}{\rho_1\alpha_1C_p}(E_{01}+BU_1)^2=0 \tag{1}$$

$$D_1\frac{d^2C_1}{dY^2}-K_1(C_1-\bar{C}_2)=0$$

Region-II

$$\rho_2\beta_{T2}g(T_2-T_{w2})+\rho_2\beta_{T2}g(C_2-\bar{C}_2)+\frac{\mu_2}{(1+\lambda_2)}\frac{d^2U_2}{dY^2}-\frac{\mu_2U_2}{\kappa}-\frac{dp}{dX}-\sigma_{e2}(E_{02}+B_0U_2)B_0=0$$

$$\frac{d^2T_2}{dY^2}+\frac{\mu_2}{\rho_2\alpha_2C_p}\left(\frac{dU_2}{dY}\right)^2+\frac{\sigma_{e2}}{\rho_2\alpha_2C_p}(E_0+BU_2)^2=0 \tag{2}$$

$$D_2\frac{d^2C_2}{dY^2}-K_2(C_2-\bar{C}_2)=0$$

Boundary interface conditions are as follows[18,19]:

$$\begin{gathered}U_1(-h_1)=0,U_2(h_2)=0,U_1(0)=U_2(0),\ \frac{\mu_1}{(1+\lambda_1)}\frac{dU_1}{dY}(0)=\frac{\mu_2}{(1+\lambda_2)}\frac{dU_2}{dY}(0)\\ T_1(-h_1)=Tw_1,\ T_2(h_2)=Tw_2,T_1(0)=T_2(0),K_1\frac{dT_1}{dY}(0)=K_2\frac{dT_2}{dY}(0)\\ C_1(-h_1)=\bar{C}_1,C_2(h_2)=\bar{C}_2,C_1(0)=C_2(0),\ D_1\frac{dC_1}{dY}(0)=D_2\frac{dC_2}{dY}(0)\end{gathered} \tag{3}$$

Corresponding to the following non-dimensional variables:

$$\begin{gathered}u_i=\frac{U_i}{U_1},\ y_i=\frac{Y_i}{h_i},\ \theta_1=\frac{T_1-T_{w2}}{T_{w1}-T_{w2}},\ \theta_2=\frac{T_2-T_{w2}}{T_{w1}-T_{w2}},\ \phi_1=\frac{C_1-\bar{C}_2}{\bar{C}_1-\bar{C}_2},\ \phi_2=\frac{C_2-\bar{C}_2}{\bar{C}_1-\bar{C}_2}\\ \Delta T=T_{w1}-T_{w2},\ \Delta\phi=\bar{C}_1-\bar{C}_2,\ {\alpha_1}^2=\frac{K_1{h_1}^2}{D_1},\ {\alpha_2}^2=\frac{K_2{h_2}^2}{D_2}\end{gathered} \tag{4}$$

$$Gr = \frac{g\beta_{T1}\Delta T {h_1}^3}{{\upsilon_1}^2},\ Gc = \frac{g\beta_{c1}\Delta T {h_1}^3}{{\upsilon_1}^2},\ Re = \frac{\overline{U_1}h_1}{\upsilon_1},\ Br = \frac{\overline{U_1}^2\mu_1}{K_1(T_{w1}-T_{w2})}$$

$$p = \frac{{h_1}^2}{\mu_1\overline{U_1}}\frac{dp}{dX}, M^2 = \frac{\sigma_{e1}{B_0}^2{h_1}^2}{\mu_1},\ E = \frac{E_{01}}{B_0\bar{u}_1}$$

Substituting the non-dimensional variables (4) into Equations (1) and (2) we get

Region-I

$$\frac{d^2u_1}{dy^2} + (1+\lambda_1)G_1\theta_1 + (1+\lambda_1)G_2\phi_1 - (1+\lambda_1)p - (1+\lambda_1)M^2[E+u_1] = 0$$

$$\frac{d^2\theta_1}{dy^2} + Br\left[\left(\frac{du_1}{dy}\right)^2 + M^2(u_1+E)^2\right] = 0 \tag{5}$$

$$\frac{d^2\phi_1}{dy^2} - {\alpha_1}^2\phi_1 = 0$$

Region-II

$$\frac{d^2u_2}{dy^2} + mh^2[nb_tG_1(1+\lambda_2)\theta_2 + nb_cG_2(1+\lambda_2)\phi_2 - M^2\sigma r(EEr+u_2)(1+\lambda_2) - p(1+\lambda_2)] = 0$$

$$\frac{d^2\theta_2}{dy^2} + Br\left(\frac{k}{m}\left(\frac{du_2}{dy}\right)^2 + M^2h^2K\sigma r(u_2+EEr)^2\right) = 0 \tag{6}$$

$$\frac{d^2\phi_2}{dy^2} - {\alpha_2}^2\phi_2 = 0$$

After the transformation of conditions at the interface and boundary Equation (3) transforms into,

$$u_1(-1) = 0, y = 1 \text{ at } y = -1, u_2(1) = 0 \text{ at } y=1 u_1(0) = u_2(0), \frac{1}{(1+\lambda_1)}\frac{du_1}{dy}(0) = \frac{1}{(1+\lambda_2)mh}\frac{du_2}{dy}(0) \text{ at } y = 0$$

$$\theta_1(-1) = 1 \text{ at } y = -1,\ \theta_2(1) = 0 \text{ at } y = 1,\ \theta_1(0) = \theta_2(0),\ \frac{d\theta_1}{dy}(0) = \frac{1}{kh}\frac{d\theta_2}{dy}(0) \text{ at } y = 0$$

$$\phi_1(-1) = 1 \text{at } y = -1, \phi_2(1) = 0 \text{ at } y = 1,\ \phi_1(0) = \phi_2(0),\ \frac{d\phi_1}{dy}(0) = \frac{d}{h}\frac{d\phi_2}{dy}(0) \text{ at } y = 0$$

where,

$$G_1 = \frac{Gr}{Re}, G_2 = \frac{Gc}{Re}, h = \frac{h_2}{h_1},\ m = \frac{\mu_1}{\mu_2},\ b_t = \frac{\beta_{T2}}{\beta_{T1}},\ b_c = \frac{\beta_{c2}}{\beta_{c1}}, n = \frac{\rho_2}{\rho_1}, d = \frac{D_2}{D_1}, Er = \frac{E_{02}}{E_{01}}, K = \frac{K_1}{K_2}, \sigma r = \frac{\sigma e_2}{\sigma e_1} \tag{7}$$

3. Method of solutions

The governing Equations (5) and (6) are solved numerically using the finite difference method subject to initial and boundary conditions given in Equation (7). Thus, the explicit finite difference method is utilized to solve the system of governing equations. The forward time central in space for u, θ, and ϕ is given as follows:

$$\frac{\partial u}{\partial y} = \frac{u_{j+1}-u_{j-1}}{2\Delta y}, \frac{\partial\theta}{\partial y} = \frac{\theta_{j+1}-\theta_{j-1}}{2\Delta y}, \frac{\partial C}{\partial y} = \frac{\phi_{j+1}-C\phi_{j-1}}{2\Delta y}, \frac{\partial^2 u}{\partial y^2} = \frac{u_{j-1}-2u_j+u_{j+1}}{\Delta y^2}, \frac{\partial^2\theta}{\partial y^2} = \frac{\theta_{j-1}-2\theta_j+\theta_{j+1}}{\Delta y^2}, \frac{\partial^2\phi}{\partial y^2} = \frac{\phi_{j-1}-2\phi_j+\phi_{j+1}}{\Delta y^2}, \phi = \phi_j, \theta = \theta_j, u = u_j \tag{8}$$

Substituting Equation (8) into Equations (5) and (6), yields the following governing equation in finite difference form:

Region-I

$$\frac{u_{1j-1} - 2u_{1j} + u_{1j+1}}{\Delta y^2} + (1+\lambda_1)G_1\theta_{1j} + (1+\lambda_1)G_2\phi_{1j} - (1+\lambda_1)p - (1+\lambda_1)M^2[E+u_{1j}] = 0$$

$$\frac{\theta_{1j-1} - 2\theta_{1j} + \theta_{1j+1}}{\Delta y^2} + Br\left[\left(\frac{u_{2j+1}-u_{2j-1}}{2\Delta y}\right)^2 + M^2(u_{1j}+E)^2\right] = 0 \tag{9}$$

$$\frac{\phi_{1j-1} - 2\phi_{1j} + \phi_{1j+1}}{\Delta y^2} - {\alpha_1}^2\phi_{1j} = 0$$

Region-II

$$\frac{u_{2j-1}-2u_{2j}+u_{2j+1}}{\Delta y^2}+mh^2[nb_tG_1(1+\lambda_2)\theta_{2j}+nb_cG_2(1+\lambda_2)\phi_{2j}-M^2\sigma r(EEr+u_2j)(1+\lambda_2)$$
$$-p(1+\lambda_2)]=0$$
$$\frac{\theta_{2j-1}-2\theta_{2j}+\theta_{2j+1}}{\Delta y^2}+Br\left(\frac{k}{m}\left(\frac{u_{2j+1}-u_{2j-1}}{2\Delta y}\right)^2+M^2h^2K\sigma r(u_{2j}+EEr)^2\right)=0 \quad (10)$$
$$\frac{\phi_{2j-1}-2\phi_{2j}+\phi_{2j+1}}{\Delta y^2}-{\alpha_2}^2\phi_{2j}=0$$

4. Result and discussion

This section highlights the influence of magnetic fields, Jeffrey fluid flow, and first-order chemical reactions on the sustainability of the system. The influence of various physical parameters on the flow variables is discussed through graphs. The implications of the findings on potential applications, such as energy generation and material processing.

From **Figure 2**, graphically, it's noted that both the velocity and thermal field's profiles grow with larger values of the viscosity ratio parameter. Physically, by raising the values of the viscosity ratio, both fields increase due to the heat absorption effect.

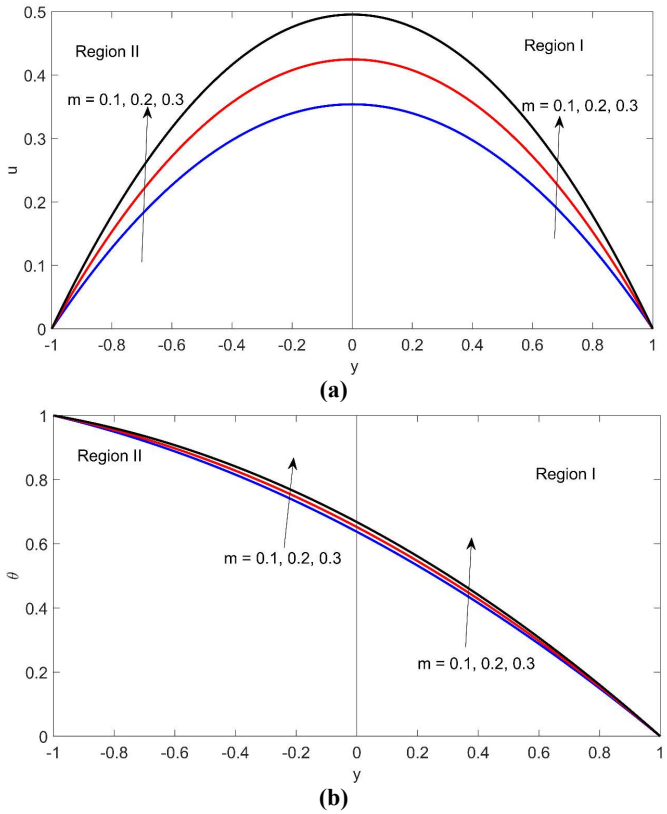

Figure 2. (a) and **(b)**, velocity and temperature profiles for different values of viscosity ratios.

From **Figure 3**, it's noted that increasing the Hartmann number recedes the velocity field profiles. Physically, as expected, rising values of M result in an increase in magnetic force that retards the motion of the fluid due to the Lorentz force. Also, it's observed that M has opposite effects in the thermal field profiles.

From **Figure 4**, graphically, it's noticed that the flow field profiles grow with higher progressive values of the width ratio parameter. Physically, increasing the width ratio enhances the flow width, and as a result, flow increases for both velocity and thermal field profiles.

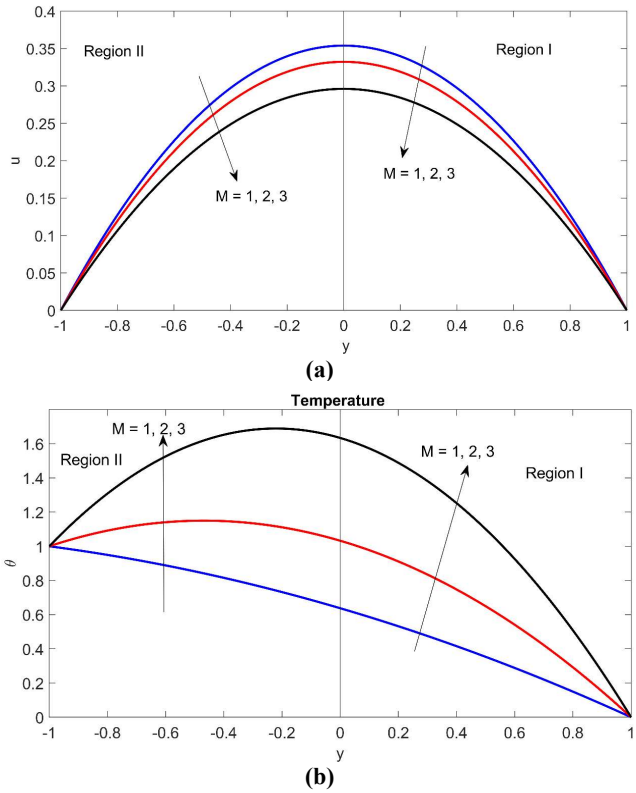

Figure 3. (a) and **(b)**, velocity and temperature profile for different values of Hartmann number.

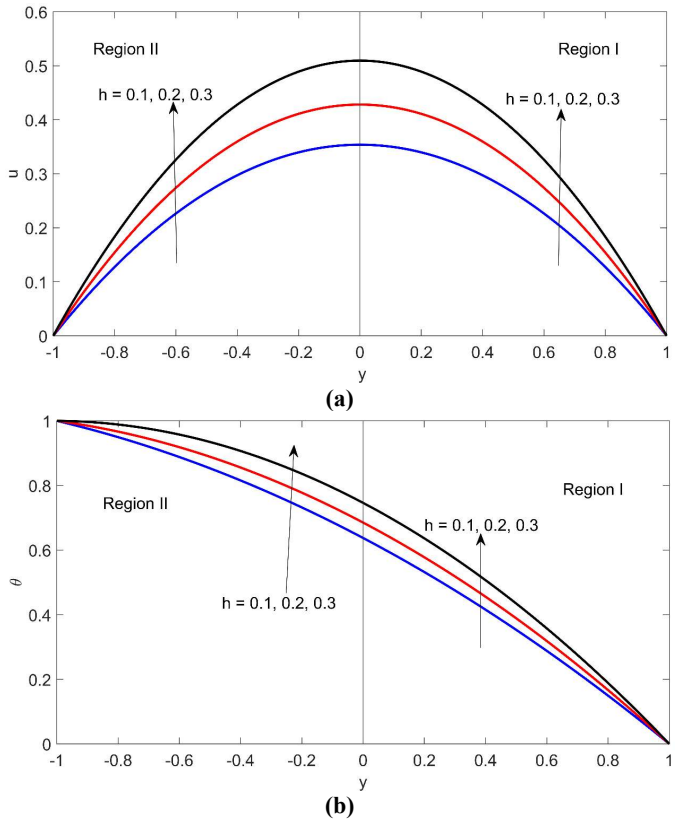

Figure 4. (a) and **(b)**, velocity and temperature profile for different values of width ratios.

From **Figure 5**, graphically, it's observed that the flow field profiles rise with higher values of the Grashof number. Physically, increasing the Grashof number results in a reduction of viscous force in the flow and thus increases the buoyancy force. As a result, it optimizes the velocity field profiles.

Figure 6 shows that an increase in the electrical load-carrying parameter increases the energy. As a result, conductivity in the fluid increases, and hence the flow is enhanced.

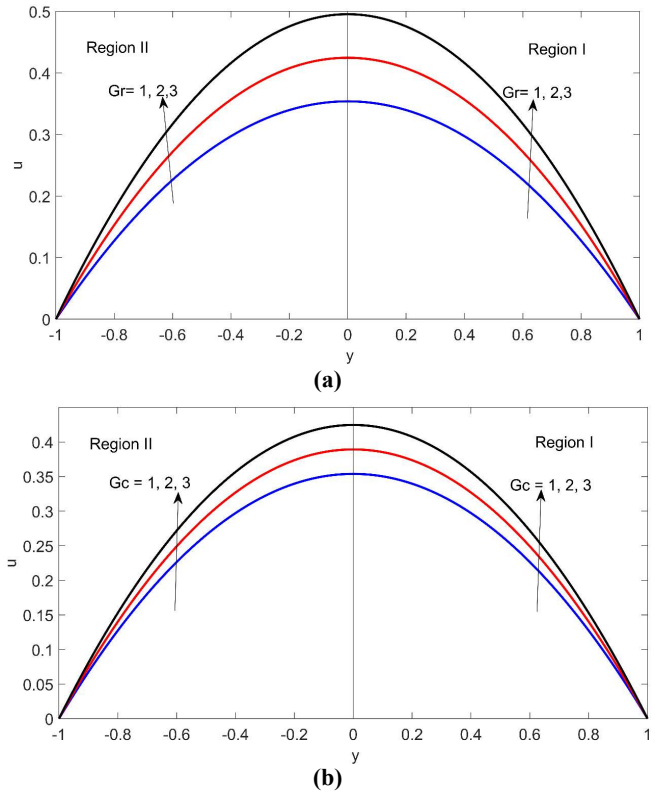

Figure 5. (a) and **(b)**, velocity profile for different values of Grashof number.

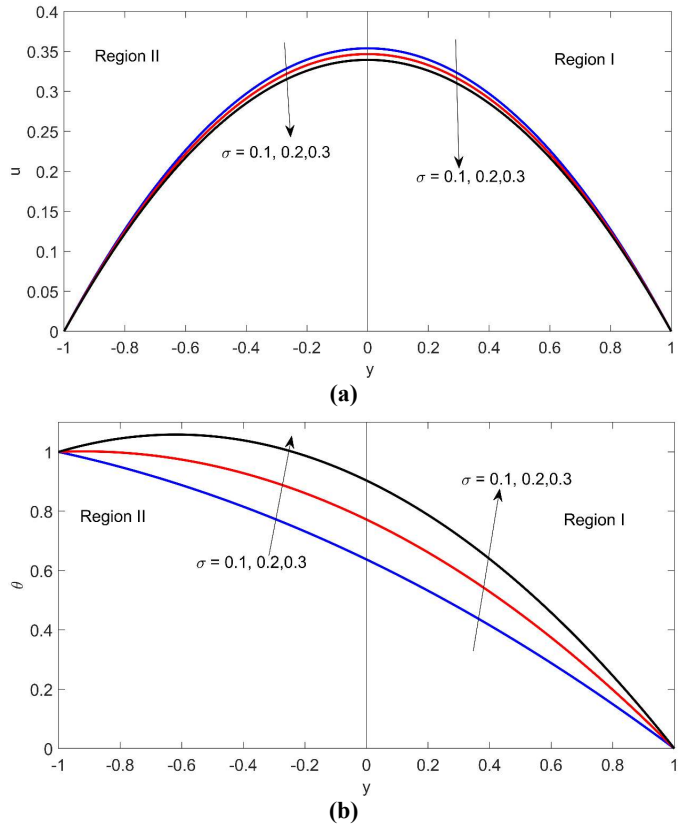

Figure 6. (a) and **(b)**, velocity and temperature profiles for different values of electrical load parameters.

Graphically, from **Figure 7**, it can be seen that the velocity field profiles recede with progressive increments of the values of the Jeffrey parameter. Physically, due to the stress relaxation property of the fluid, the flow is suppressed.

Figure 8 shows that the thermal field profiles increase with higher values of k. Physically, increasing the conductivity results in an increase of the flow field due to thermo-property.

Figure 9 shows that the velocity field profiles recede with higher values of the electrical conductivity parameter. Physically, rising values of E retard the flow fields. Also, it's observed that for different electric circuits with different electricity, it enhances the thermal field profiles.

Figure 10 shows that the concentration decreases with higher values of destructive chemical reaction parameters. Physically, increasing the chemical reaction parameter increases the solute molecules, and as a result, the diffusion process decreases, so the flow field decreases.

From **Figure 11**, it's observed that the velocity field and thermal field profiles grow with progressive increments of the Brinkman number. Physically, rising Brinkman number Br enhances the flow due to buoyancy and electrical field.

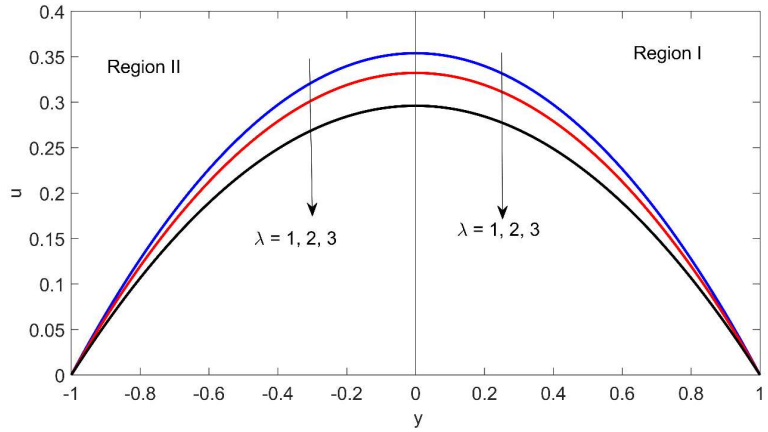

Figure 7. Velocity profile for different values of Jeffrey parameter.

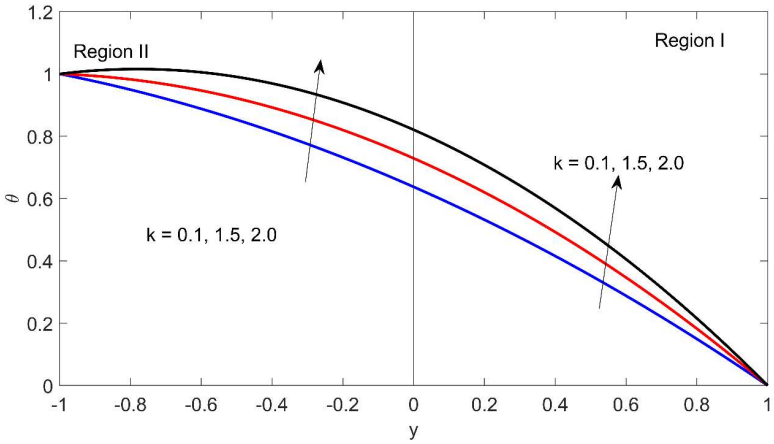

Figure 8. Temperature profile for different values of k.

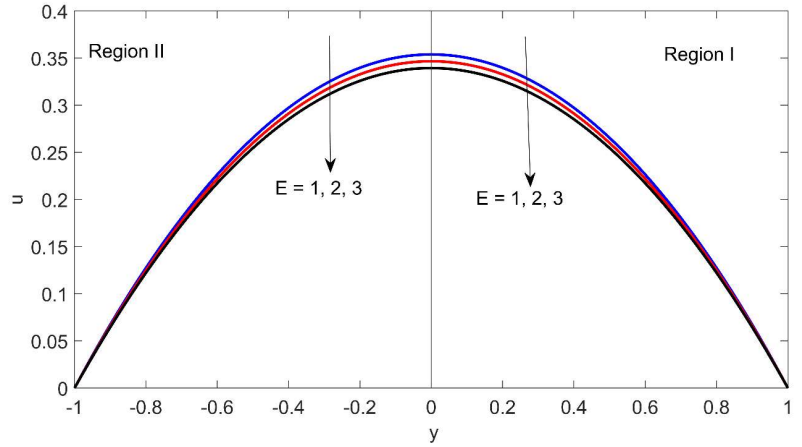

(a)

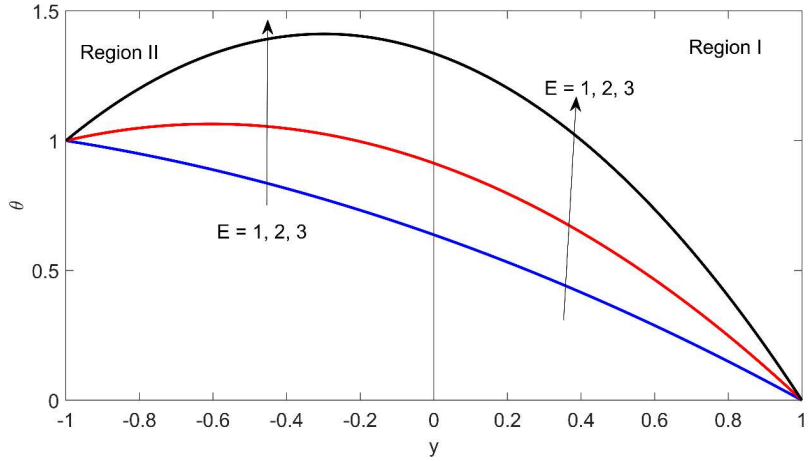

(b)

Figure 9. (a) and **(b)**, velocity and temperature profile for different values of electrical conductivity.

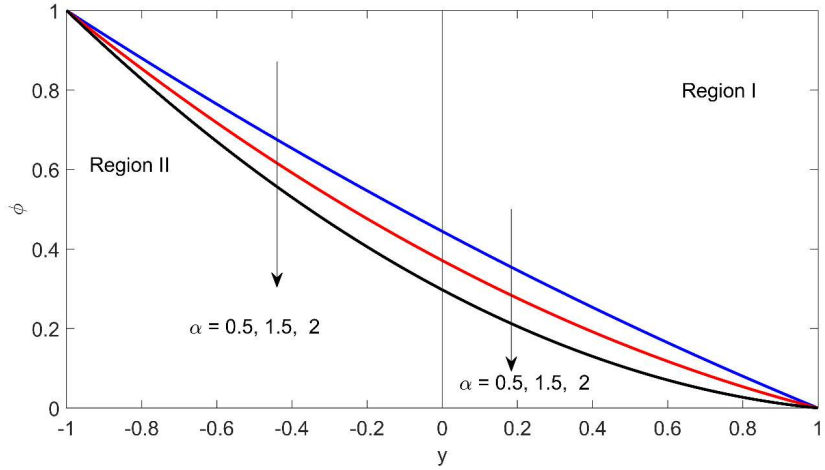

Figure 10. Concentration profile for different values of chemical reaction parameter.

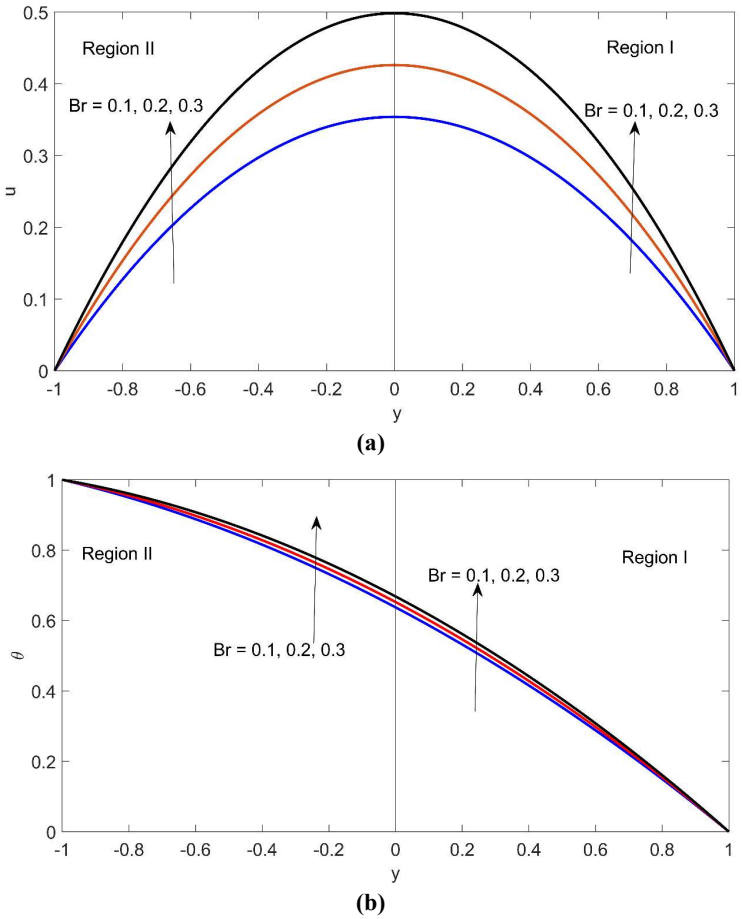

Figure 11. **(a)** and **(b)**, velocity and temperature profile for different values of Brinkman number.

5. Conclusions

This research paper provides insights into the fluid sustainability of electrically conducting MHD fluids with Jeffrey fluid flow and first-order chemical reactions. The combination of magnetohydrodynamics and the unique rheological properties of Jeffrey fluid opens new avenues for optimizing engineering processes and enhancing sustainability in various applications. The major findings of this study are summarized as follows:

(i) The velocity field profiles are enhanced with Gr, Gc, Br, h, and m and declined with λ, σ, E, and M.

(ii) The Species concentration field profiles decline with larger values of α.

(iii) The thermal field profiles are enhanced with Br, E, k, m, σ, h, and M.

Nomenclature

b_t: The ratio of Thermal expansion coefficient, β_{T2}/β_{T1}

b_c: The ratio of concentration expansion coefficient β_{c2}/β_{c1}

g: Acceleration due to gravity

E: Electric field load parameter $(\frac{E_{01}}{B_0}\overline{u_1})$

E_{01}, E_{02}: Applied electric fields

Er: Applied electric filed ratios

σ_e: Electrical conductivity

Br: Brinkmann number $\frac{\mu_1 \overline{U_1}^2}{k_1}(T_{w1} - T_{w2})$

GR_T: Thermal Grashof number

GR_c: Mass Grashof number

G_1: The ratio of Grashof to Reynolds numbers, $\frac{Gr}{Re}$

G_2: The ratio of Grashof to Reynolds numbers, $\frac{Gc}{Re}$

λ_1, λ_2: Jeffrey parameter

h: Width ratio h_2/h_1

h_1, h_2: Height of Region-I, II

d: diffusion coefficient ratio $(\frac{D_2}{D_1})$

D_1, D_2: diffusion coefficient

K: Thermal conductivities ratios, $\frac{K_1}{K_2}$

K_1, K_2: Thermal conductivity in Region-I, II

n: Micro-rotational velocity

m: Ratio of viscosities, μ_1/μ_2

Re: Reynolds number

P: Pressure Gradient $(\frac{h_1^2}{\mu_1 \overline{U_1}}\frac{dp}{dX})$

T_0: Average temperature

T: Temperature

T_{W1}, T_{W2}: Temperature of the boundaries

C_1, C_2: Concentrations of the boundaries

$\overline{C_1}$, $\overline{C_2}$: Reference concentrations

U: Velocity

U_0: Average velocity

X, Y: Space co-ordinates

Greek symbols:

β: thermal expansion coefficient

μ: Viscosity

α_1, α_2: Chemical reaction parameters

ρ_1, , ρ_2: Density of Region-I, II

ΔT: Temperature difference

ΔC: Difference in concentration

υ_1, υ_2: Kinematic viscosities

ϕ_1, ϕ_2: concentrations in Region-I,II

θ: Dimensionless temperature

Subscript:

1, 2 represent Region-I, II respectively.

Author contributions

Conceptualization, SK and JM; methodology, JM; software, JM; validation, SK and JM; formal analysis, JM; investigation, SK; resources, SK; data curation, SK; writing—original draft preparation, SK; writing—review and editing, JM; visualization, SK; supervision, SK; project administration, SK; funding acquisition, SK. All authors have read and agreed to the published version of the manuscript.

Conflict of interest

The authors declare no conflict of interest.

References

1. Narsimha Reddy B, Maddileti P, Chesnea C. Stagnation point on MHD boundary layer flow of heat and mass transfer over a non-linear stretching sheet with effect of Casson nanofluid. *International Journal of Modelling and Simulation* 2023. doi: 10.1080/02286203.2023.2286420
2. Noh J, Jekal S, Kim J, et al. Vivid-colored electrorheological fluids with simultaneous enhancements in color clarity and electro-responsivity. *Journal of Colloid and Interface Science* 2024; 657: 373–383. doi: 10.1016/j.jcis.2023.11.183
3. Sedki A, Qahiti R. Unsteady magnetohydrodynamic radiative Casson nanofluid within chemically reactive flow over a stretchable surface with variable thickness through a porous medium. *Energies* 2023; 16(23): 7776. doi: 10.3390/en16237776
4. Venkateswarlu B, Chavan S, Joo SW, Kim SC. Entropy analysis of electromagnetic trihybrid nanofluid flow with temperature-dependent viscosity in a Darcy-Forchheimer porous medium over a stretching sheet under convective conditions. *Journal of Molecular Liquids* 2024; 393: 123660. doi: 10.1016/j.molliq.2023.123660
5. Guedri K, Khan A, Gul T, et al. Thermally dissipative flow and entropy analysis for electromagnetic trihybrid nanofluid flow past a stretching surface. *ACS Omega* 2022; 7(37): 33432–33442. doi: 10.1021/acsomega.2c04047
6. Govindarajan A, Lakshmipriya S. Effect of soret on two immiscible fluids through vertical parallel plates in the presence of chemical reaction with radiation. *AIP Conference Proceedings* 2020; 2277(1): 030006. doi: 10.1063/5.0025801
7. Sandeep N, Sulochana C, Isaac Lare A. Stagnation-point flow of a Jeffrey nanofluid over a stretching surface with induced magnetic field and chemical reaction. *International Journal of Engineering Research in Africa* 2015; 20: 93–111. doi: 10.4028/www.scientific.net/JERA.20.93
8. Raju CSK, Sandeep N, Gnaneswara Reddy M. Effect of nonlinear thermal radiation on 3D Jeffrey fluid flow in the presence of homogeneous-heterogeneous reactions. *International Journal of Engineering Research in Africa* 2015; 21: 52–68. doi: 10.4028/www.scientific.net/JERA.21.52
9. Rashidi MM, Ali M, Freidoonimehr N, et al. Mixed convective heat transfer for MHD viscoelastic fluid flow over a porous wedge with thermal radiation. *Advances in Mechanical Engineering* 2014; 6: 735939. doi: 10.1155/2014/735939
10. Nield DA, Kuznetsov AV. The Cheng-Minkowycz problem for natural convective boundary-layer flow in a porous medium saturated by a nanofluid. *International Journal of Heat and Mass Transfer* 2009; 52(25–26): 5792–5795. doi: 10.1016/j.ijheatmasstransfer.2009.07.024
11. Kuznetsov AV, Nield DA. The Cheng-Minkowycz problem for natural convective boundary layer flow in a porous medium saturated by a nanofluid: a revised model. *International Journal of Heat and Mass Transfer* 2013; 65: 682–685. doi: 10.1016/j.ijheatmasstransfer.2013.06.054
12. Halim NA, Sivasankaran S, Noor NFM. Active and passive controls of the Williamson stagnation nanofluid flow over a stretching/shrinking surface. *Neural Computing and Applications* 2016; 28: 1023–1033. doi: 10.1007/s00521-016-2380-y
13. Hayat T, Muhammad T, Alsaedi A, Alhuthali MS. Magnetohydrodynamic three-dimensional flow of viscoelastic nanofluid in the presence of nonlinear thermal radiation. *Journal of Magnetism and Magnetic Materials* 2015; 385: 222–229. doi: 10.1016/j.jmmm.2015.02.046

14. Malvandi A, Ganji DD, Pop I. Laminar filmwise condensation of nanofluids over a vertical plate considering nanoparticles migration. *Applied Thermal Engineering* 2016; 100: 979–986. doi: 10.1016/j.applthermaleng.2016.02.061
15. Hayat T, Aziz A, Muhammad T, et al. On magnetohydrodynamic flow of second grade nanofluid over a convectively heated nonlinear stretching surface. *Advanced Powder Technology* 2016; 27(5): 1992–2004. doi: 10.1016/j.apt.2016.07.00
16. Halim NA, Ul Haq R, Noor NFM. Active and passive controls of nanoparticles in Maxwell stagnation point flow over a slipped stretched surface. *Meccanica* 2017; 52: 1527–1539. doi: 10.1007/s11012-016-0517-9
17. Hayat T, Aziz A, Muhammad T, Alsaedi A. Active and passive controls of Jeffrey nanofluid flow over a nonlinear stretching surface. *Results in Physics* 2017; 7: 4071–4078. doi: 10.1016/j.rinp.2017.10.028
18. Kalyan S, Sharan A, Chamkha AJ. Heat and mass transfer of two immiscible flows of Jeffrey fluid in a vertical channel. *Heat Transfer* 2022; 52(1): 267–288. doi: 10.1002/htj.22694
19. Thanesh Kumar K, Kalyan S, Kandagal M, et al. Influence of heat generation/absorption on mixed convection flow field with porous matrix in a vertical channel. *Case Studies in Thermal Engineering* 2023; 47: 103049. doi: 10.1016/j.csite.2023.103049